Excitons and narrow bands determine the optical properties of cesium bismuth halides

Sebastian Rieger, Bernhard J. Bohn, Markus Döblinger, Alexander F. Richter, Yu Tong, Kun Wang, Peter Müller-Buschbaum, Lakshminarayana Polavarapu, Linn Leppert, Jacek K. Stolarczyk, and Jochen Feldmann

Phys. Rev. B **100**, 201404 — Published 20 November 2019

DOI: 10.1103/PhysRevB.100.201404

Excitons and narrow bands determine the optical properties of cesium bismuth halides

Sebastian Rieger,[1,2] Bernhard J. Bohn,[1,2] Markus Döblinger,[3] Alexander F. Richter,[1,2] Yu Tong,[1,2] Kun Wang,[4] Peter Müller-Buschbaum,[4,5] Lakshminarayana Polavarapu,[1,2] Linn Leppert,[6,*] Jacek K. Stolarczyk,[1,2,*] and Jochen Feldmann[1,2,*]

[1]*Chair for Photonics and Optoelectronics, Nano-Institute Munich, Department of Physics, Ludwig-Maximilians-Universität (LMU), Königinstr. 10, 80539 Munich, Germany*

[2]*Nanosystems Initiative Munich (NIM) and Center for NanoScience (CeNS), Schellingstr. 4, 80799 Munich, Germany*

[3]*Department of Chemistry, Ludwig-Maximilians-Universität (LMU), Butenandtstr. 5–13 (E), 81377 Munich, Germany*

[4]*Lehrstuhl für Funktionelle Materialien, Physik Department, Technische Universität München, James-Franck-Strasse 1, 85747 Garching, Germany.*

[5]*Heinz Maier-Leibnitz Zentrum (MLZ), Technische Universität München, Lichtenbergstr. 1, 85748 Garching, Germany*

[6]*Institute of Physics, University of Bayreuth, 95440 Bayreuth, Germany*

Abstract

We study the optical properties of $Cs_3Bi_2I_9$ nanoplatelets using a combination of first-principles density functional theory, GW-Bethe-Salpeter equation calculations and spectroscopic experiments. We show that the material exhibits flat bands and hence high effective masses. This manifests itself in the lowest energy transition in the absorption spectrum arising from excitons with a high binding energy of 300 meV and Bohr radius smaller than 6 nm. Due to the indirect band gap, electrons and holes are efficiently separated in reciprocal space and recombine slowly across the band gap, leading to very weak photoluminescence. Our results resolve inconsistencies in previous studies on $Cs_3Bi_2I_9$ and lay ground for further work on applications of this material, reliant on charge separation.

Keywords: first principles calculations, band structure, exciton, transient absorption spectroscopy, perovskite, bismuth, nanocrystal

Alternatives for lead halide perovskites with advantageous optical properties are needed to address the toxicity of lead.[1] Bismuth is an appealing candidate because of the isoelectronic structure of the Bi^{3+} cation with Pb^{2+}, featuring a $6s^2$ lone electron pair and comparable ionic radii.[2,3] To maintain charge balance, the aliovalent replacement of Pb^{2+} with Bi^{3+} requires a vacancy ordered structure $A_3Bi_2X_9$ in which every third Bi^{3+} cation is missing.[2,4,5] For cesium or methylammonium (MA) as the A-site cation, the remaining BiX_6 units then rearrange to form pairs of face-sharing octahedra.[6] Such low-dimensional perovskite-like structures exhibit strong absorption in the visible range, reasonable electron and hole mobilities of 4.3 $cm^2 \cdot V^{-1} \cdot s^{-1}$ and 1.7 $cm^2 \cdot V^{-1} \cdot s^{-1}$, respectively and estimated electron and hole lifetimes of about 11 μs.[7] A $Cs_3Bi_2I_9$-based solar cell with 3.2% efficiency was recently reported.[8] With carrier mobility and lifetimes greater than expected from the isolated nature of the $Bi_2I_9^{3-}$ bioctahedra in the crystal structure, the crystal structure can be treated not as 0D, but *quasi*-0D. This raises questions about the strength of the electronic coupling between the bioctahedra, as well as about the efficiency of charge separation in real and reciprocal space. Furthermore, the optical properties of these materials are subject to debate. The absorption spectra of $MA_3Bi_2I_9$ and $Cs_3Bi_2I_9$ exhibit a distinct peak at around 2.5 eV, directly arising at the absorption onset.[4,6] In prior conflicting studies the attribution of this peak has been inconsistent, with one explanation involving a bound electron-hole pair.[8] Alternatively, the peak is assigned to the band edge, and its isolation attributed to the splitting of the conduction band into separate sub-bands due to spin-orbit coupling.[9] Per analogy with lead halide perovskites, the latter effect is expected to manifest itself strongly in $Cs_3Bi_2I_9$.[10]

Colloidal semiconductor nanocrystals (NCs) exhibit unique properties when the crystal size is close to or below the exciton Bohr radius, *e.g.,* an increase in band gap or in exciton binding energy due to a reduced dielectric screening.[11-13] The *quasi*-0D character of the $Bi_2I_9^{3-}$ bioctahedra in $Cs_3Bi_2I_9$ - placing the material between the regimes of molecular and solid crystals[14] - complicates the description and remains poorly investigated. In this context, $Cs_3Bi_2I_9$ provides a convenient platform to study the inherently reduced dimensionality of Bi-based perovskites.[15,16] Here, we investigate nanoplatelets of $Cs_3Bi_2I_9$ using a combination of first-principles density functional theory (DFT) calculations and the GW plus Bethe-Salpeter equation (GW-BSE) approach with time-integrated and time-resolved optical measurements.[17-19] The weakly coupled bioctahedral subunits are found to give rise to flat bands in the band structure, visible in the optical absorption spectrum. Furthermore, we demonstrate that the prominent peak in the absorption spectrum arises from Coulombic electron-hole interactions and reflects a bound exciton with a high 300 meV binding energy as a consequence of the high effective masses. We attribute the very weak photoluminescence (PL) to the separation of electrons and holes in reciprocal space and subsequent slow radiative recombination across the indirect band gap. We conclude that despite its *quasi*-0D crystal structure this non-toxic and stable material has promising properties for applications reliant on efficient charge separation. [8] The experimental procedures of the sample preparation[20] and characterization are detailed in the Supplemental Material.[21]

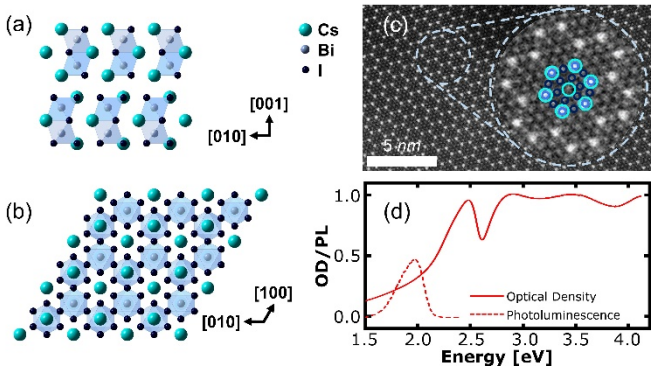

FIG. 1. 3D model of the *P6₃/mmc* crystal structure (a) along the [100] direction showing spatially separated bioctahedral units and (b) along the [001] direction illustrating the hexagonal arrangement of the octahedral columns. (c) HAADF-STEM image of $Cs_3Bi_2I_9$ along the [001] direction, magnified in the inset with the

elemental assignment of the atomic columns. (d) Optical density (solid line) and photoluminescence spectrum (dashed line) of $Cs_3Bi_2I_9$.

In the *P6₃/mmc* crystal structure, reported earlier for $Cs_3Bi_2I_9$[4,6] and confirmed in XRD (see Figure S1) and EDX studies (see Figure S2), each unit cell consists of two pairs of face-sharing halide octahedra, containing one Bi^{3+} ion in each octahedron (see Figure 1a). The bioctahedra are separated by the Cs^+ cations and aligned to form a layered structure. [4,6,15,22,23] Projected along the hexagonal axis, the arrangement of the bioctahedral units forms a honeycomb pattern (cf. Figure 1b) which can be seen clearly in the high resolution STEM image in high-angle annular dark field (HAADF) mode (Figure 1c). This allows for an assignment of the columns of atoms (see inset), owing to the uniform alignment of the nanoplatelets lying flat on the surface, such that the electron beam passes the crystal precisely in the [001] direction (see Figure S3).

The extinction spectrum of the $Cs_3Bi_2I_9$ nanoplatelets (see Figure 1d) shows a slow absorption onset with a distinct peak at 2.5 eV (495 nm), as well as several less prominent and spectrally broader peaks at higher energies, namely at 2.91 eV, 3.45 eV and a further rise in absorbance starting above 4.0 eV. The spectrum acquired with an integrating sphere setup in order to eliminate the contribution of scattering shows a much sharper absorption onset, with virtually no tail at lower energies (see Figure S4). Both, the absorption spectra acquired for much larger and much smaller crystals do not differ from the spectrum of the nanoplatelets, implying that quantum confinement by the nanocrystal size does not play a significant role.[4,15] In contrast to lead halide perovskite nanocrystals, the $Cs_3Bi_2I_9$ nanoplatelets exhibit extremely weak photoluminescence with a peak at 2.0 eV upon excitation at 2.64 eV (470 nm, see dotted line in Figure 1d) indicating a significant Stokes shift with respect to the absorption onset.

In order to deduce the assignment and the character of electronic transitions corresponding to the peaks in the absorption and emission spectra, we performed DFT calculations to determine the band structure of $Cs_3Bi_2I_9$. We used the experimental crystal structure and generalized gradient approximation of Perdew, Burke, and Ernzerhof (PBE) as implemented in the VASP code,[24,25] including spin-orbit coupling (SOC) self-consistently (see Supplemental Material for details[21,26,27]). The calculated bands are plotted in Figure 2a, with the contributions of I p orbitals highlighted in Figure S5a and those of Bi s and p orbitals in Figure S5b, respectively. The bands form an indirect gap with the minimum of the conduction band at the Γ point and the maxima of the valence band at the M, K and H points of the Brillouin zone. Similar to lead-based perovskites, Cs-derived orbitals do not contribute to the states near the band gap. In this context, the weak dispersion of the bands in k-space and the appearance of minibands, as seen in Figure 2a, substantiates the treatment of $Cs_3Bi_2I_9$ as a *quasi*-0D crystal structure with weak electronic coupling between the symmetry-inequivalent bioctahedral units. Furthermore, due to SOC the conduction band is split into two sub-bands corresponding to total angular momentum J = 1/2 (CB1) and J = 3/2 (CB2), separated by an energy gap of ~ 1 eV at the Γ point. The total width of the CB1 band is $\Delta_{CB1} \approx 0.5$ eV at the M point. The states in the conduction band have pure *p*-character as they are formed by hybridization of Bi 6p and I 5p orbitals. In contrast, the valence band has mixed orbital character. Its two highest energy bands are composed of Bi 6s- and I 5p-derived states, covering a very narrow energy region, although there are only few orbitals with Bi 6s character contributing to the states close to the band edge. All the deeper bands within several eVs below the band edge are formed by Bi p- and I p-derived states, similar to the bottom of the conduction band.

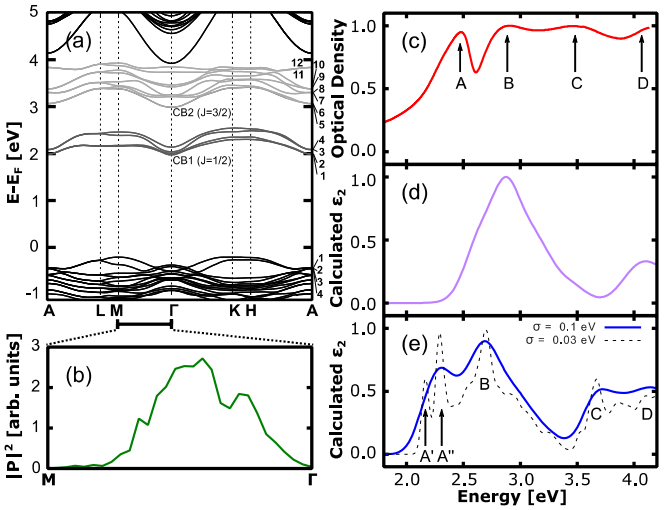

FIG. 2. (a) The DFT-PBE+SOC band structure of $Cs_3Bi_2I_9$. Conduction bands are shifted so as to reproduce the G_0W_0@PBE+SOC band gap.[28] The individual bands in the VB and CB are labelled from 1 to 4 and 1 to 12, respectively. The conduction band is split into two sub-bands with a total angular momentum J = 1/2 (CB1, dark grey) and J = 3/2 (CB2, light grey) (b) Transition dipole matrix elements ($|P|^2$) for direct transitions from the highest energy valence band to the lowest energy conduction band calculated within the independent particle approximation. (c) The experimental extinction spectrum of $Cs_3Bi_2I_9$ with labels (A-D) for the individual peaks compared with the imaginary part of the dielectric function calculated using the *ab initio* GW-Bethe-Salpeter equation approach, (d) without and (e) with consideration of electron-hole interactions with a line broadening of 0.1 eV (solid line) and 0.03 eV (dashed line) including labels (A' and A") for the underlying distinct contributions to the excitonic peak.

The crystal symmetry and orbital character of the conduction and valence bands restrict the number of dipole-allowed transitions. We therefore calculated the transition dipole matrix elements along the high-symmetry line M to Γ in the independent particle approximation (see Figure 2b). The resulting dipole matrix elements are zero at the high symmetry points M and Γ, but increase away from these points. The highest energy valence bands are relatively flat, suggesting that the density of occupied states at the band edge is non-zero for only a narrow range of energy. Furthermore, only in this range, the bands possess a partial *s*-character (see Figure S5). This should result in energetically distinct transitions from the top of the valence band to the two narrow sub-bands CB1 and CB2, respectively. These transitions, rather than bound excitons, have been linked to the prominent peak A in the absorption spectrum in prior studies.[9] We explicitly tested this conjecture, by calculating the frequency-dependent linear absorption spectrum of $Cs_3Bi_2I_9$ using *ab initio* Green's function-based many-body perturbation theory. [29,30] In order to calculate the excitation spectrum including electron-hole interactions, we solve the Bethe-Salpeter equation (BSE) for the correlated electron-hole amplitude as implemented in the BerkeleyGW package,[31] which interpolates the electron-hole kernel matrix elements and quasiparticle energies from a coarse to a fine k-point grid. We used a fine grid of 8x8x2 k-points, and included 16 valence and 16 conduction bands in the solution of the BSE. The BSE matrix elements are constructed based on a previous G_0W_0@PBE+SOC calculation, i.e., the zeroth-order Green's function G_0 and screened Coulomb interaction W_0 are obtained from DFT-PBE including SOC self-consistently (see SI for further computational details). [21,32-35] The experimental spectrum (Figure 2c) is directly compared with the calculated absorption spectra of $Cs_3Bi_2I_9$ without and with electron-hole interactions displayed in Figure 2d and e, respectively. When electron-hole interactions are ignored, there are just two strong peaks at 2.9 eV and 4.1 eV in the spectrum. The 1.2 eV energy difference between these dominant peaks is significantly larger than any separation of the distinct peaks between A and D in the experimental spectrum, suggesting that these peaks correspond to transitions to the CB1 and CB2, respectively. However, the inclusion of electron-hole interactions not only, and expectedly, red-shifts the dominant absorption peak, but also gives rise to a new peak originating from bound electron-hole pairs. Importantly, the position of this emergent peak is in good agreement with the experimental position of the distinct peak A and supports the identification of the

latter as excitonic, in contrast to earlier reports.[9,36] A further GW-BSE calculation of the absorption spectrum with smaller line broadening (see Figure 2e) reveals that this peak originates from two distinct bound excitonic transitions. The exciton binding energy of the lowest energy exciton extracted from the theoretical data is ~230 meV, in reasonable agreement with the exciton binding energy of 295 eV obtained from the experimental absorption spectrum using Elliott's model (see Figure S6),[37] as detailed in the Supplemental Material.[21] Using this procedure, the band-to-band transition onset is found to lie at 2.75 eV, which corroborates the conclusion that the main peak at 2.75 eV in the computed spectra corresponds to a band gap transition. The experimental spectrum of $Cs_3Bi_2I_9$ (Fig. 2c) exhibits four distinct peaks (A to D). Based on our calculated spectra, peak B can be assigned to transitions from the valence band edge to CB1 near the L, M, K or H points. The width of the peak, $\Delta_{abs} \approx 0.6$ eV, agrees well with the bandwidth of the states contributing to this transition. Finally, the absorption onset starting at below 3.5 eV (peak C and D) corresponds to transitions from the valence band to CB2. The only discrepancy between the experimental and computed extinction spectra is the depth of the minimum between the peaks attributed to transitions from the valence band to CB1 and to CB2, which are more pronounced and deeper in the calculated spectrum. We attribute this difference to scattering contributions in the measured spectrum. After subtraction of these contributions, assuming linear scaling of scattering with the photon energy, we achieve very good agreement between the spectra also at energies above 3 eV (see Figure S7).

The high exciton binding energy of ~300 meV likely stems from confinement in the *quasi*-0D bioctahedral units because the cesium layers separating the bioctahedral units only hybridize in bands several eVs off the band gap reducing the coupling between the bioctahedra.[9] Based on a hydrogenic model, we have estimated the exciton Bohr radius to be ~2 nm in [001] direction and ~6 nm in [100] direction (see details in the Supplemental Material[21]). This implies the presence of weak electronic coupling between the bioctahedra and is consistent with the appearance of flat bands in the band structure. Hence, the character of the material, with properties intermediate between those typical for a semiconductor and a molecular crystal substantiates the qualifier *quasi*-0D for this structure. The size of the exciton Bohr radius of less than 6 nm is much smaller than the thickness of the nanoplatelets suggesting that no morphology-related quantum confinement is expected for the synthesized $Cs_3Bi_2I_9$ nanoplatelets.[14]

In contrast to lead halide perovskites, the $Cs_3Bi_2I_9$ nanoplatelets reported here have extremely weak PL, despite the high exciton binding energy of ~300 meV. The very small radiative rate may be explained using the calculated band structure which demonstrates that $Cs_3Bi_2I_9$ is an indirect semiconductor with a conduction band minimum at the Γ point and the valence band maximum at the M point, with similar maxima at the K and H points. Moreover, the direct energy transitions at the Γ point are dipole forbidden (Figure 2b).

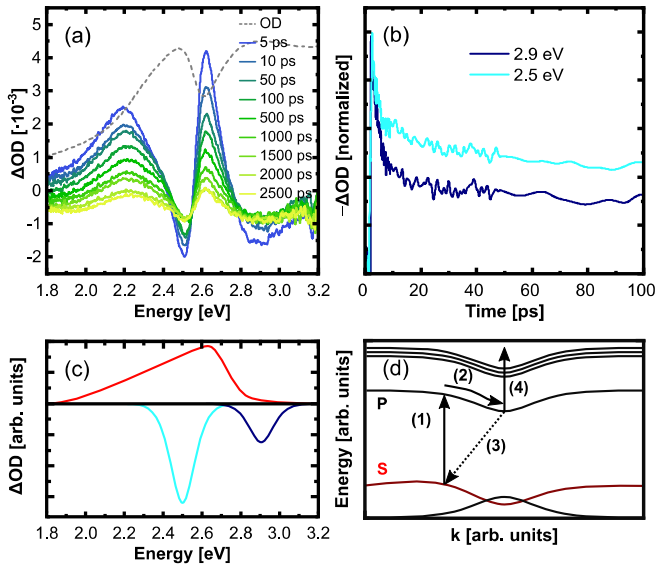

FIG. 3. (a) Differential absorption spectra for an excitation wavelength of 350 nm and a pump power of 250 μW (250 nJ per pulse) for different time delays between the pump and the probe pulse (5 ps to 2500 ps). The time-integrated spectrum is plotted for reference (grey dashed line). (b) Scheme of the three underlying contributions to the Differential absorption spectrum: photo-induced absorption (red), exciton

bleaching (indigo) and band edge bleaching (blue). (c) Time-dependent intensity of the normalized exciton (2.5 eV) and band edge (2.9 eV) bleaching signals from (a). (d) Scheme of involved optical transitions: absorption from the ground state (1), relaxation of electrons to the conduction band minimum (2), indirect recombination (3) and photo-induced absorption to higher bands (4).

The only allowed transitions are originating from states around the M point (as well as H and K points) in the valence band. There is no local minimum at neither of these reciprocal coordinates of the conduction band.[38] In fact, at the region of the highest transition probability, shown in Figure 2b, there is a gradient towards the conduction band minimum at the Γ point in the CB1. This means that upon excitation, the electrons will quickly relax to this minimum. From there the direct recombination is forbidden, which favors the indirect transition with a hole remaining near the M point of the valence band. Such a transition would be expected to result in weak and strongly Stokes shifted PL, indeed observed experimentally.

To verify this mechanism of charge separation in reciprocal space, we investigated the carrier transfer with femtosecond transient absorption spectroscopy (see Figure 3a). In this technique, the transient signal is proportional to the sum of contributions of the electrons and holes, which makes it particularly suitable to monitor the presence of charge carriers. The nanocrystals were excited with laser pulses at 3.54 eV (350 nm) and the differential spectra were acquired with a broadband probe pulse at different probe time delays. As a reference, Figure 3a also shows the static spectrum. There are two peaks in the differential spectra with negative ΔOD at the energies of the exciton (2.5 eV) and the direct band gap (2.9 eV) which can be understood on the basis of phase-space filling by the pump-excited carriers occupying the excitonic and band edge states. This bleaches the corresponding transitions for subsequent incident photons of the probe pulse. The minima are distinct although not very strong. This is probably due to an overlap with a very broad photoinduced absorption signal that reduces the intensity of the negative peaks. This broad positive ΔOD signal spanning almost the entire range depicted schematically in Figure 3b was only observed when the sample was excited above the band edge of CB1, suggesting that it arises from the excitation of electrons from the CB1 to higher bands.

The kinetic traces of the relaxation of the ΔOD peaks at 2.5 eV and 2.9 eV, normalized by the maximum depth of the bleaching, are plotted in Figure 3c. They exhibit a rapid decay of the bleaching signal in the first 10 ps to around 50% of its initial intensity, followed by a very slow relaxation. These results agree very well with the mechanism elucidated from the analysis of the band structure. They corroborate the assumption that the electrons quickly relax to the minimum at the Γ point (initial decay to around half intensity), but the holes remain at the VB maxima in reciprocal space (remaining half of the signal), schematically depicted in Figure 3d. This is consistent with the suggested strong electron-phonon coupling in $Cs_3Bi_2I_9$ [39] and other bismuth-based perovskites.[40] As expected, the slow recombination across the indirect band gap is power-dependent (see Figure S8) while the fast relaxation seems to be independent. In effect, the electrons and holes separate and may only recombine through an indirect transition dominated by the non-radiative channels of recombination. According to our G_0W_0@PBE+SOC band structure calculations, the energy of this indirect transition (2.18 eV) is much lower than the excitation energy near the M point, in good agreement with the observed strong Stokes shift observed for the PL spectrum (see Figure 1d). These observations are also consistent with the extremely low reported photoluminescence quantum yield of 0.017%[5,15] and support the attribution of the higher quantum yield, reported earlier for ultrasmall $MA_3Bi_2I_9$ nanocrystals, to surface defect emission.[41] Presence of non-radiative, possibly (surface-)defect-mediated recombination channels is indicated by the results of additional time-resolved PL measurements which suggest short PL lifetimes on the ps time scale despite the indirect band gap (see Figure S9). At the same time, the observation that the bleaching of the excitonic and

band gap transitions do not decay beyond the initial ~50% at least until 3 ns (the longest delay measured) also shows an efficient charge separation in reciprocal space, an advantageous property for photovoltaic or photocatalytic applications.

In summary, we have used *ab initio* DFT and GW-BSE calculations to elucidate the electronic structure and demonstrate the excitonic character of the distinct peak in the absorption spectra at 2.5 eV of $Cs_3Bi_2I_9$. Combining the theoretical predictions with static and time-resolved spectroscopic measurements, we show that the very weak PL originates from the forbidden character of the lowest energy direct transition and the very fast separation of charge carriers in reciprocal space. The electrons relax to the conduction band minimum at the Γ point so that only slow indirect transitions are allowed. Consequently, the radiative recombination pathway is outcompeted by non-radiative channels leading to very low PL quantum yield, despite the localization of the excitons in the bioctahedral units of the crystals lattice. The effective charge separation, consistent with long reported lifetimes, suggests that these *quasi*-0D materials are an appealing and potentially viable option for applications in which this property is desired, such as solar cells or photocatalysis.

Acknowledgements

This work was supported by the Bavarian State Ministry of Science, Research, and Arts through the grant "Solar Technologies go Hybrid (SolTech)", by the China Scholarship Council (Y.T. & K.W.) and by the Deutsche Forschungsgemeinschaft (DFG) through the excellence cluster "e-conversion". LL acknowledges financial support by the Elite Network Bavaria and computational resources provided by the Bavarian Polymer Institute and DFG via SFB840. Portions of this work were also supported by National Energy Research Scientific Computing Center (NERSC), a U.S. Department of Energy Office of Science User Facility operated under Contract No. DE-AC02-05CH11231.

* linn.leppert@uni-bayreuth.de, jacek.stolarczyk@physik.uni-muenchen.de, feldmann@lmu.de

References

[1] J.-P. Correa-Baena, M. Saliba, T. Buonassisi, M. Grätzel, A. Abate, W. Tress, and A. Hagfeldt, Promises and challenges of perovskite solar cells, Science **358**, 739 (2017).

[2] F. Giustino, and H. J. Snaith, Toward Lead-Free Perovskite Solar Cells, ACS Energy Lett. **1**, 1233-1240 (2016).

[3] C. N. Savory, A. Walsh, and D. O. Scanlon, Can Pb-Free Halide Double Perovskites Support High-Efficiency Solar Cells?, ACS Energy Lett. **1**, 949-955 (2016).

[4] B.-W. Park, B. Philippe, X. Zhang, H. Rensmo, G. Boschloo, and E. M. Johansson, Bismuth based hybrid perovskites A3Bi2I9 (A: methylammonium or cesium) for solar cell application, Adv. Mater. **27**, 6806-6813 (2015).

[5] K. K. Bass, L. Estergreen, C. N. Savory, J. Buckeridge, D. O. Scanlon, P. I. Djurovich, S. E. Bradforth, M. E. Thompson, and B. C. Melot, Vibronic Structure in Room Temperature Photoluminescence of the Halide Perovskite Cs3Bi2Br9, Inorg. Chem. **56**, 42-45 (2017).

[6] A. J. Lehner, D. H. Fabini, H. A. Evans, C.-A. Hébert, S. R. Smock, J. Hu, H. Wang, J. W. Zwanziger, M. L. Chabinyc, and R. Seshadri, Crystal and Electronic Structures of Complex Bismuth Iodides A3Bi2I9 (A= K, Rb, Cs) Related to Perovskite: Aiding the Rational Design of Photovoltaics, Chem. Mater **27**, 7137-7148 (2015).

[7] K. M. McCall, Z. Liu, G. Trimarchi, C. C. Stoumpos, W. Lin, Y. He, I. Hadar, M. G. Kanatzidis, and B. W. Wessels, α-Particle Detection and Charge Transport Characteristics in the A3M2I9 Defect Perovskites (A = Cs, Rb; M = Bi, Sb), ACS Photonics **5**, 3748-3762 (2018).

[8] F. Bai, Y. Hu, Y. Hu, T. Qiu, X. Miao, and S. Zhang, Lead-free, air-stable ultrathin Cs3Bi2I9 perovskite nanosheets for solar cells, Sol. Energy Mater. Sol. Cells **184**, 15-21 (2018).

[9] M. Pazoki, M. B. Johansson, H. Zhu, P. Broqvist, T. Edvinsson, G. Boschloo, and E. M. J. Johansson, Bismuth Iodide Perovskite Materials for Solar Cell Applications: Electronic Structure, Optical

Transitions, and Directional Charge Transport, J. Phys. Chem. C **120**, 29039-29046 (2016).
[10] J. Even, L. Pedesseau, J.-M. Jancu, and C. Katan, Importance of Spin–Orbit Coupling in Hybrid Organic/Inorganic Perovskites for Photovoltaic Applications, J. Phys. Chem. Lett. **4**, 2999-3005 (2013).
[11] J. A. Sichert, Y. Tong, N. Mutz, M. Vollmer, S. Fischer, K. Z. Milowska, R. Garcia Cortadella, B. Nickel, C. Cardenas-Daw, and J. K. Stolarczyk, Quantum size effect in organometal halide perovskite nanoplatelets, Nano Lett. **15**, 6521-6527 (2015).
[12] V. A. Hintermayr, A. F. Richter, F. Ehrat, M. Döblinger, W. Vanderlinden, J. A. Sichert, Y. Tong, L. Polavarapu, J. Feldmann, and A. S. Urban, Tuning the Optical Properties of Perovskite Nanoplatelets through Composition and Thickness by Ligand-Assisted Exfoliation, Adv. Mater. **28**, 9478-9485 (2016).
[13] V. A. Hintermayr, L. Polavarapu, A. S. Urban, and J. Feldmann, Accelerated Carrier Relaxation through Reduced Coulomb Screening in Two-Dimensional Halide Perovskite Nanoplatelets, ACS Nano **12**, 10151-10158 (2018).
[14] M.-G. Ju, J. Dai, L. Ma, Y. Zhou, and X. C. Zeng, Zero-Dimensional Organic–Inorganic Perovskite Variant: Transition between Molecular and Solid Crystal, J. Am. Chem. Soc. **140**, 10456-10463 (2018).
[15] Y. Zhang, J. Yin, M. R. Parida, G. H. Ahmed, J. Pan, O. M. Bakr, J.-L. Brédas, and O. F. Mohammed, Direct-Indirect Nature of the Bandgap in Lead-Free Perovskite Nanocrystals, J. Phys. Chem. Lett. (2017).
[16] L. Lian, G. Zhai, F. Cheng, Y. Xia, M. Zheng, J. Ke, M. Gao, H. Liu, D. Zhang, L. Li, J. Gao, J. Tang, and J. Zhang, Colloidal synthesis of lead-free all-inorganic cesium bismuth bromide perovskite nanoplatelets, CrystEngComm **20**, 7473-7478 (2018).
[17] M. S. Hybertsen, and S. G. Louie, Electron correlation in semiconductors and insulators: Band gaps and quasiparticle energies, Phys. Rev. B **34**, 5390-5413 (1986).
[18] M. Rohlfing, and S. G. Louie, Electron-Hole Excitations in Semiconductors and Insulators, Phys. Rev. Lett. **81**, 2312-2315 (1998).
[19] M. Rohlfing, and S. G. Louie, Electron-hole excitations and optical spectra from first principles, Phys. Rev. B **62**, 4927-4944 (2000).
[20] Y. Tong, F. Ehrat, W. Vanderlinden, C. Cardenas-Daw, J. K. Stolarczyk, L. Polavarapu, and A. S. Urban, Dilution-Induced Formation of Hybrid Perovskite Nanoplatelets, ACS Nano **10**, 10936-10944 (2016).
[21] See Supplemental Material at http://link.aps.org for experimental and computational details.
[22] S. Melnikova, and A. Zaitsev, Ferroelectric phase transition in Cs 3 Bi 2 I 9, Phys. Solid State **39**, 1652-1654 (1997).
[23] S. Oz, J.-C. Hebig, E. Jung, T. Singh, A. Lepcha, S. Olthof, F. Jan, Y. Gao, R. German, and P. H. van Loosdrecht, Zero-dimensional (CH3NH3)3Bi2I9 perovskite for optoelectronic applications, Sol. Energy Mater. Sol. Cells **158**, 195-201 (2016).
[24] J. P. Perdew, K. Burke, and M. Ernzerhof, Generalized Gradient Approximation Made Simple, Phys. Rev. Lett. **77**, 3865-3868 (1996).
[25] G. Kresse, and J. Furthmüller, Efficient iterative schemes for ab initio total-energy calculations using a plane-wave basis set, Phys. Rev. B **54**, 11169-11186 (1996).
[26] G. Kresse, and J. Hafner, Norm-conserving and ultrasoft pseudopotentials for first-row and transition elements, J. Phys. Condens. Matter **6**, 8245-8257 (1994).
[27] J. Klimeš, M. Kaltak, and G. Kresse, Predictive GW calculations using plane waves and pseudopotentials, Phys. Rev. B **90**, 075125 (2014).
[28] L. Leppert, T. Range, and J. B. Neaton, Towards predictive band gaps for halide perovskites: Lessons from one-shot and eigenvalue self-consistent GW, Phys. Rev. Mater. **3**, 103803 (2019).
[29] S. Albrecht, L. Reining, R. Del Sole, and G. Onida, Ab Initio Calculation of Excitonic Effects in the Optical Spectra of Semiconductors, Phys. Rev. Lett. **80**, 4510-4513 (1998).
[30] A. L. Fetter, and J. D. Walecka, *Quantum theory of many-particle systems*. (McGraw-Hill, 1971).
[31] J. Deslippe, G. Samsonidze, D. A. Strubbe, M. Jain, M. L. Cohen, and S. G. Louie, BerkeleyGW: A massively parallel computer package for the calculation of the quasiparticle and optical properties of materials and nanostructures, Comput. Phys. Commun. **183**, 1269-1289 (2012).
[32] F. Aryasetiawan, and O. Gunnarsson, The GW method, Rep. Prog. Phys. **61**, 237 (1998).
[33] P. Giannozzi, S. Baroni, N. Bonini, M. Calandra, R. Car, C. Cavazzoni, D. Ceresoli, G. L. Chiarotti, M. Cococcioni, I. Dabo, A. Dal Corso, S. de Gironcoli, S. Fabris, G. Fratesi, R. Gebauer, U. Gerstmann, C. Gougoussis, A. Kokalj, M. Lazzeri, L. Martin-Samos, N. Marzari, F. Mauri, R. Mazzarello, S. Paolini, A. Pasquarello, L. Paulatto, C. Sbraccia, S. Scandolo, G. Sclauzero, A. P. Seitsonen, A. Smogunov,

P. Umari, and R. M. Wentzcovitch, QUANTUM ESPRESSO: a modular and open-source software project for quantum simulations of materials, J. Phys. Condens. Matter **21**, 395502 (2009).
[34] J. Deslippe, G. Samsonidze, M. Jain, M. L. Cohen, and S. G. Louie, Coulomb-hole summations and energies for GW calculations with limited number of empty orbitals: A modified static remainder approach, Phys. Rev. B **87**, 165124 (2013).
[35] D. R. Hamann, Optimized norm-conserving Vanderbilt pseudopotentials, Phys. Rev. B **88**, 085117 (2013).
[36] R. L. Z. Hoye, R. E. Brandt, A. Osherov, V. Stevanović, S. D. Stranks, M. W. B. Wilson, H. Kim, A. J. Akey, J. D. Perkins, R. C. Kurchin, J. R. Poindexter, E. N. Wang, M. G. Bawendi, V. Bulović, and T. Buonassisi, Methylammonium Bismuth Iodide as a Lead-Free, Stable Hybrid Organic–Inorganic Solar Absorber, Chem. Eur. J. **22**, 2605-2610 (2016).
[37] R. J. Elliott, Intensity of Optical Absorption by Excitons, Phys. Rev. **108**, 1384-1389 (1957).
[38] H. C. Liu, C. Y. Song, A. Shen, M. Gao, Z. R. Wasilewski, and M. Buchanan, GaAs/AlGaAs quantum-well photodetector for visible and middle infrared dual-band detection, Appl. Phys. Lett. **77**, 2437-2439 (2000).
[39] K. M. McCall, C. C. Stoumpos, S. S. Kostina, M. G. Kanatzidis, and B. W. Wessels, Strong Electron–Phonon Coupling and Self-Trapped Excitons in the Defect Halide Perovskites A3M2I9 (A = Cs, Rb; M = Bi, Sb), Chem. Mater. **29**, 4129-4145 (2017).
[40] R. Kentsch, M. Scholz, J. Horn, D. Schlettwein, K. Oum, and T. Lenzer, Exciton Dynamics and Electron–Phonon Coupling Affect the Photovoltaic Performance of the Cs2AgBiBr6 Double Perovskite, J. Phys. Chem. C **122**, 25940-25947 (2018).
[41] M. Leng, Z. Chen, Y. Yang, Z. Li, K. Zeng, K. Li, G. Niu, Y. He, Q. Zhou, and J. Tang, Lead-Free, Blue Emitting Bismuth Halide Perovskite Quantum Dots, Angew. Chem. Int. Ed. **55**, 15012-15016 (2016).